REPORT DOCUMENTATION PAGE

AFRL-SR-AR-TR-04-

0298

1. REPORT DATE (DD-MM-YYYY) 15-05-2004	2. REPORT TYPE: final	3. DATES COVERED (From - To) 10/1/2004

4. TITLE AND SUBTITLE
Effects of Scale-Hierarchy in *Ordered* Electro-Active Polymer Nanocomposites

5a. CONTRACT NUMBER

5b. GRANT NUMBER F49620-03-1-0105

5c. PROGRAM ELEMENT NUMBER

6. AUTHOR(S) David L. Carroll

5d. PROJECT NUMBER

5e. TASK NUMBER

5f. WORK UNIT NUMBER

7. PERFORMING ORGANIZATION NAME(S) AND ADDRESS(ES)

Clemson University
Department of Materials Science
Clemson SC 29630

8. PERFORMING ORGANIZATION REPORT NUMBER

9. SPONSORING / MONITORING AGENCY NAME(S) AND ADDRESS(ES)
AFOSR/NL
4015 Wilson Blvd, Room 713
Arlington, VA 22203-1954
c/o Dr. Charles Y-C Lee

10. SPONSOR/MONITOR'S ACRONYM(S)
AFOSR

11. SPONSOR/MONITOR'S REPORT NUMBER(S)

12. DISTRIBUTION / AVAILABILITY STATEMENT

Approve for Public Release:Distribution Unlimited

13. SUPPLEMENTARY NOTES

14. ABSTRACT

Electroactive nanocomposites are generally composed of a "minority" nanophase and a majority-phase host. Interaction between the phases is three fold: exchange of charge, mediation of radiative energy, and morphological based on energy minimization. The *meso*-structure of the nanophase can strongly influence the properties of the composite to the point of being totally dissimilar to the original pure organic. This program was intended to introduce levels of order from studies of *fractally connected* to fully coordinated assembly.

15. SUBJECT TERMS

16. SECURITY CLASSIFICATION OF:			17. LIMITATION OF ABSTRACT	18. NUMBER OF PAGES	19a. NAME OF RESPONSIBLE PERSON
a. REPORT	b. ABSTRACT	c. THIS PAGE		19	David Carroll
					19b. TELEPHONE NUMBER (Include area code) 336 758 5508

Performance report • F49620-03-1-0105 • "Effects of Scale-Hierarchy in *Ordered* Electro-Active Polymer Nanocomposites" • final

PROGRAM OVERVIEW

Goals: 1) Examination of fundamental polymer-carbon nanotube interactions in the diffuse random loading regime.
2) Introduction of *meta*-architectures in the host phase and in the nanophase.
3) Introduction of novel device platforms that more efficiently utilize the properties of carbon nanotube – electroactive polymer nanocomposites.

Statement: Electroactive nanocomposites are generally composed of a "minority" nanophase and a majority-phase host. Interaction between the phases is three fold: exchange of charge, mediation of radiative energy, and morphological based on energy minimization. The *meso*-structure of the nanophase can strongly influence the properties of the composite to the point of being totally dissimilar to the original pure organic. This program was intended to introduce levels of order from studies of *fractally connected* to fully coordinated assembly.

SUMMARY OF ACCOMPLISHMENTS

Random PVDF – CNT nanocomposites were first reported in this program. It has been demonstrated that nanocomposites of SWNTs with PVDF exhibited several important phenomena: percolation thresholds significantly below theoretical, a 100% increase in the piezo-response to a given displacement, and a 150% increase in pyroelectric coefficient. These striking results are shown in figure 1.

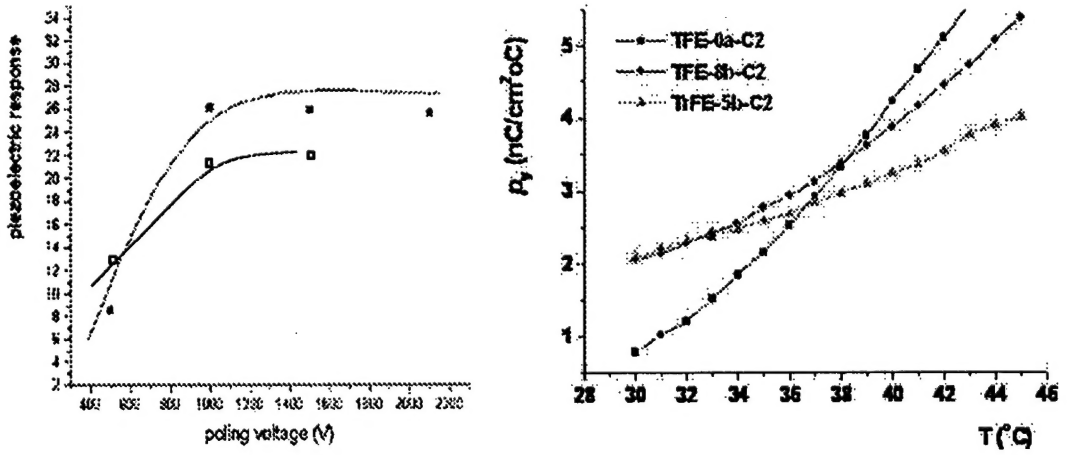

Figure 1: Left) Piezoelectric response for a specific displacement as a function of poling. The red is the nanocomposite. Right) The pyroelectric coefficient as a function of the nanocomposite. Different copolymers are presented. The black is the pure polymer.

Details
Poly(vinylidene fluoride-co-hexafluoropropylene)
Molecular weight :454,000
Melting Temperature:160°C
Glass Transition:78°C
Melt Index:3.5-7.5g/10 min
(230°C, 12.5kg)

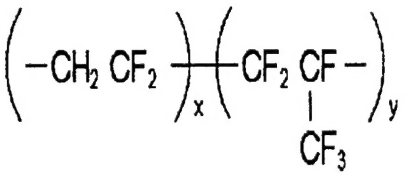

Using XRD is has been shown that the majority polymorph of the pure PVDF system is *alpha*-phase (in agreement with literature) and the piezo- pyro- phase is *beta*-phase as shown in figure 2.

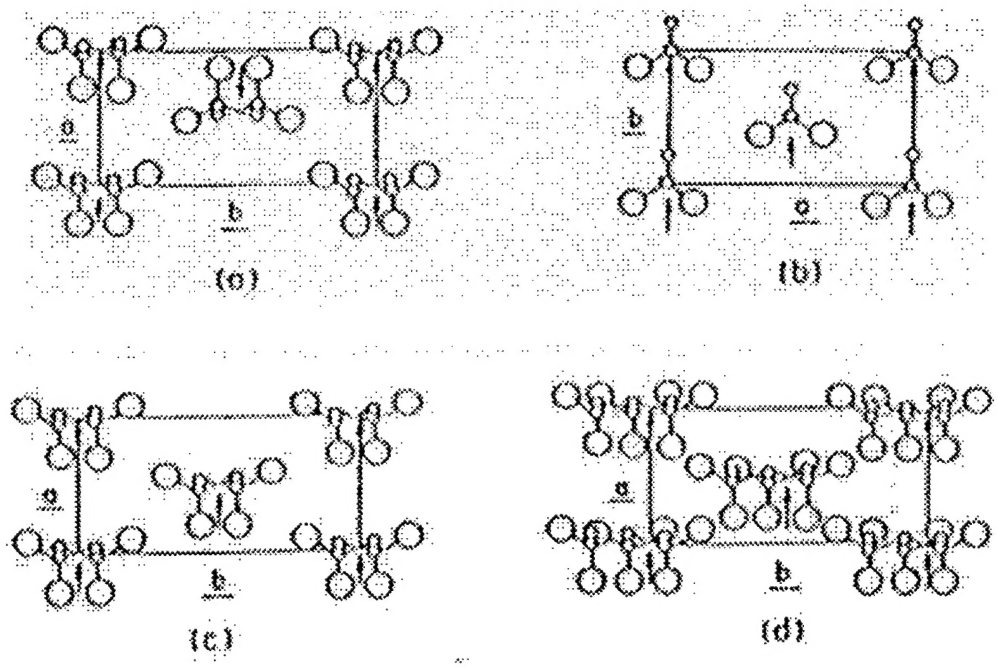

Figure 2: The polymorphs of PVDF. (a) alpha phase (b) beta phase. The delta and gamma phases below also occur in small amounts.

We have shown that carbon nanotubes induce heterogenous nucleation of crystal formation and alter the alpha to beta phase volume ratios in favor of the beta phase. To understand how the tube diameter and surface treatment (ie. surface energy of the tubes) will effect the formation of alpha polymorph, HIPCO (1.4 nm tubes), MWNTs, (20 nm tubes), arc grown (1.2 nm tubes), and fluorinated HIPCO tubes were used to determine maximum alpha phase formation. Figure 3 shows these results comparing the peak heights of alpha and beta phases from decomposed XRD peaks.

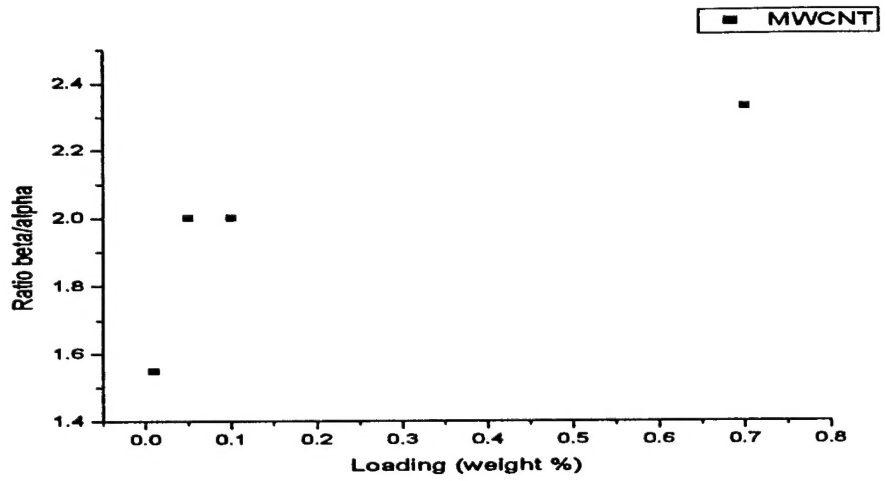
MWCNT
Ratio beta/alpha
2.4
2.2
2.0
1.8
1.6
1.4
0.0
0.1
0.2
0.3
0.4
0.5
0.6
0.7
0.8
Loading (weight %)

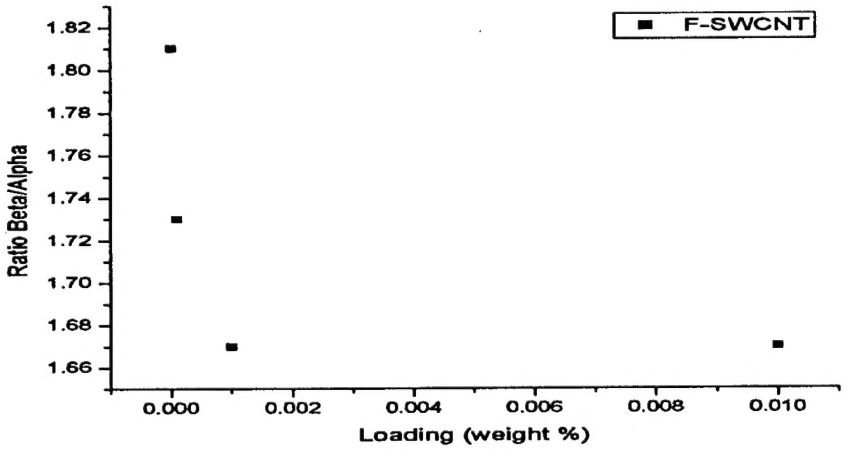
F-SWCNT
Ratio Beta/Alpha
1.82
1.80
1.78
1.76
1.74
1.72
1.70
1.68
1.66
0.000
0.002
0.004
0.006
0.008
0.010
Loading (weight %)

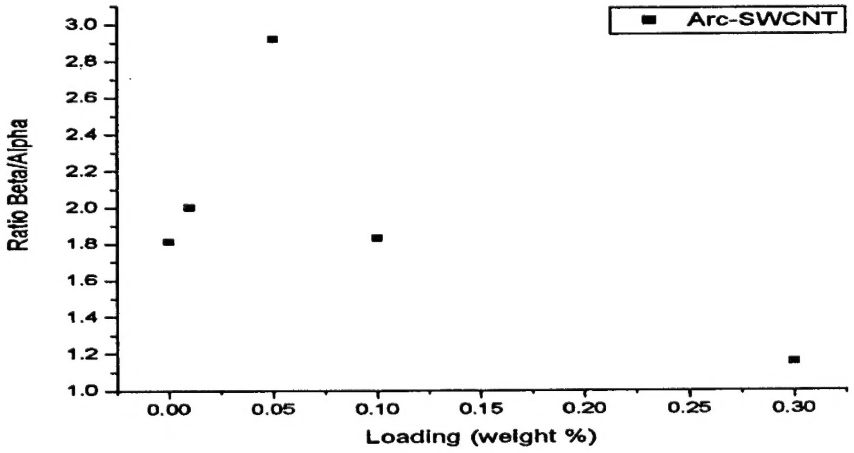
Arc-SWCNT
Ratio Beta/Alpha
3.0
2.8
2.6
2.4
2.2
2.0
1.8
1.6
1.4
1.2
1.0
0.00
0.05
0.10
0.15
0.20
0.25
0.30
Loading (weight %)

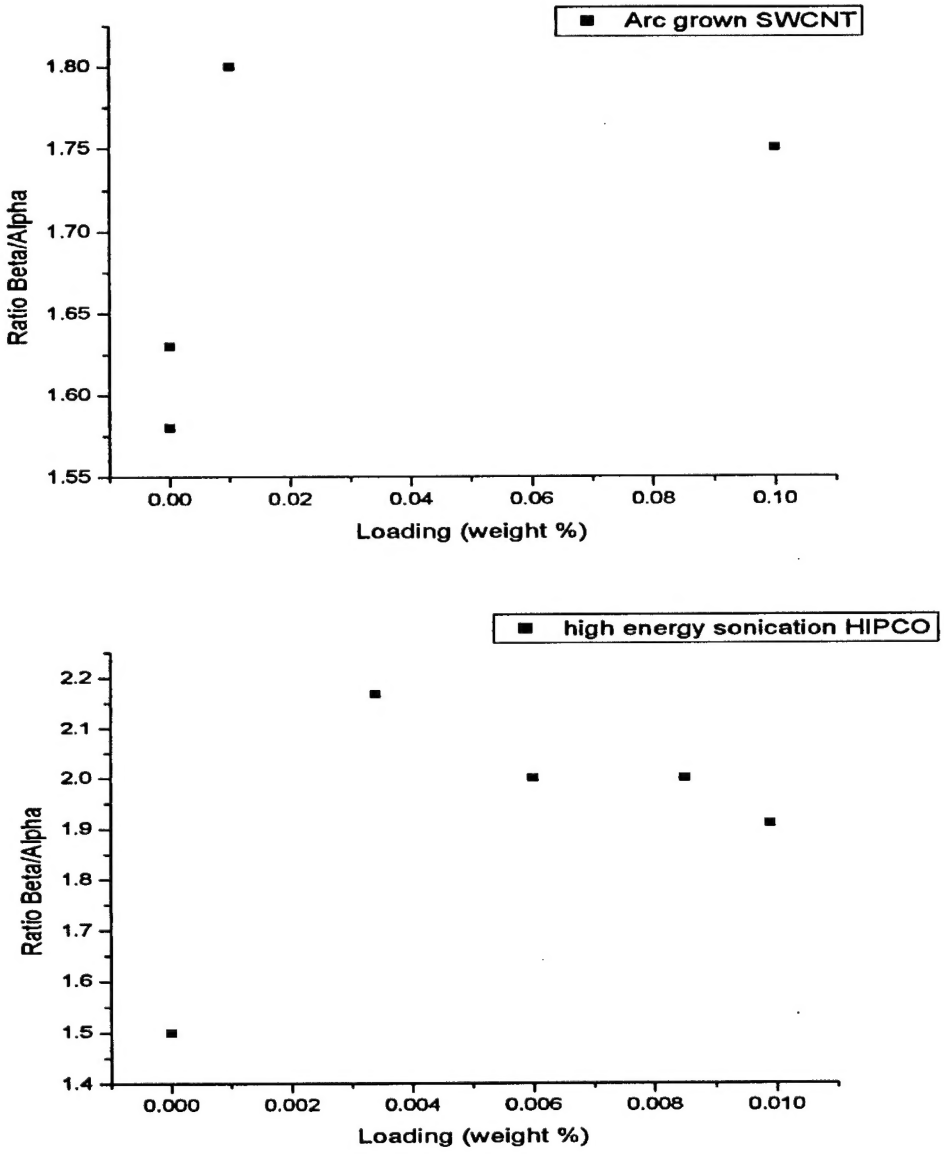

Figure 3: Notice that the beta to alpha ratio depends strongly on surface functionality as well as tube diameter indicating that this effect is morphology related and likely driven by surface energy effects.

This study shows that the alpha peak to beta peak ratio is very sensitive to the nanotube diameter and the nanotube surface treatment assuming that the overall level of bundling in the system is the same (shown earlier by optical scattering). More importantly, there occur maxima in the peak ratios (ie. In the volume percentage of alpha phase), at specific loadings, as given in the figure above.

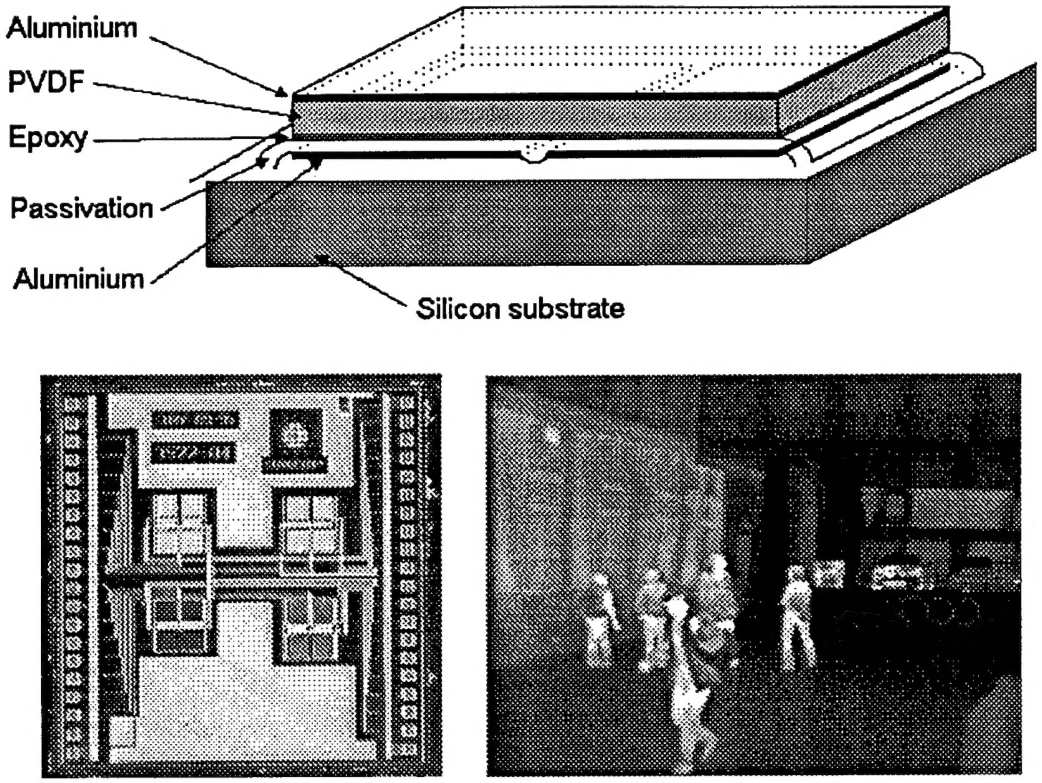

Figure 4: A PVDF based thermal imager taken from literature. Our nanocomposite will be inserted into this device using the same pixel format as shown left below.

Applications: We are currently working toward the integration of this new material into standard PVDF thermal imaging systems. Figure 4 below is taken from literature and is a thermal imaging system with PVDF as the active pyroelectric. The pyroelectric coefficient is a minimum of 2 times smaller than our current material. Thus, we anticipate significantly enhanced imaging at longer wavelengths using the nanocomposite. One patent has been grant provisional status and we are working with a small start up company (Tetramer Technologies Inc. Pendleton SC) for transfer of these results into marketplace.

CTNs based on P3OT multiple heterojunction devices (taken in part from interim report)

An area of promising application for CTN is photovoltaics. Following our original work in CNT-EAP composites for thin film devices, it was decided to optimize device design for the insertion of the nanocomposite. Forrest (Princeton) has recently demonstrated a "multiple heterojunction" device using small molecules.

Extension: To use this design with carbon nanotubes, the design had to be extended to polymeric materials. Shown below in figure 5, is the device we have constructed based on Forrest's original work. The device functions by allowing the photo-generation of

electron hole pairs in both layers. On the cathode side, holes are shunted into the PEDOT layer. On the anode side, electrons are shunted into the PEDOT layer. Thus the electrons and holes transferred to the cathode and anode can be extracted. The fullerenes were added to increase electron transfer out of the layer.

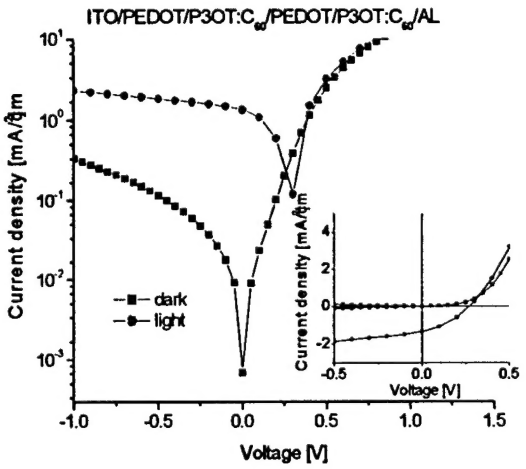

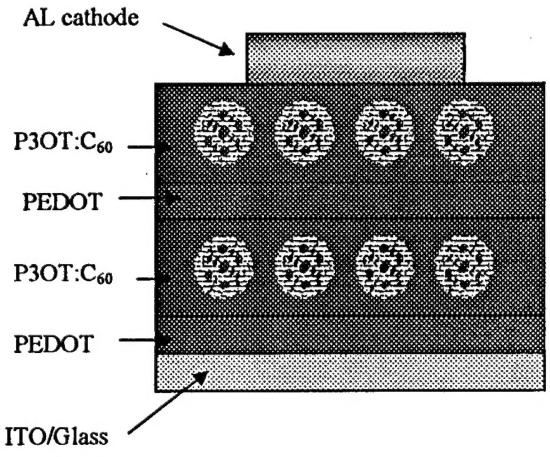

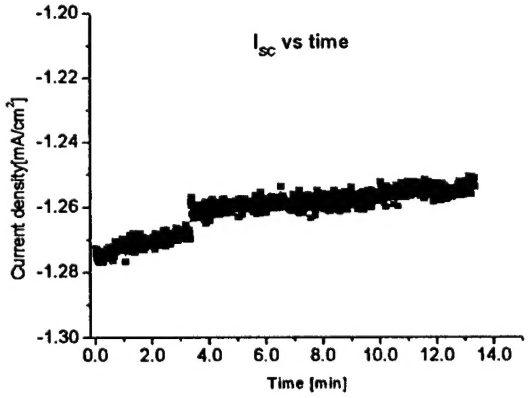

Figure 5: top right, we have made multiple heterojunction device from polymers for the first time. Top left, the performance of this device is impressive even without the nanocomosites. External conversion efficiency of the example here is 2.3 %. Bottom left, the current stability in these devices is also drastically improved.

The device shown achieved 2.3 % conversion eff. using an AM1.5g standard. Nanosilver particles will be added to increase the scattering within the device and carbon nanotubes will be added to increase PEDOT mobility. These improvements are expected to raise the eff.significantly.

Lifetime studies

We reported recently extended lifetime of organic devices employing nanocomposites. Specifically, it was found that both light emitting devices and organic photovoltaics

exhibit "unusual" resistance to degradation for operating in air. Naturally, resistance to oxidation has the potential to be quite significant and therefore merits close examination. *Extension:* To quantify the degradation of organic devices using nanocomposites a simple set of experiments that directly measured operating lifetimes were performed. Sets of organic light emitting diodes (ITO/PEDOT/PFO/Alq_3/LiAl) were placed in a glovebox and current/brightness were monitored for a given bias over some time. Shown in figure 6 are the present results of those tests.

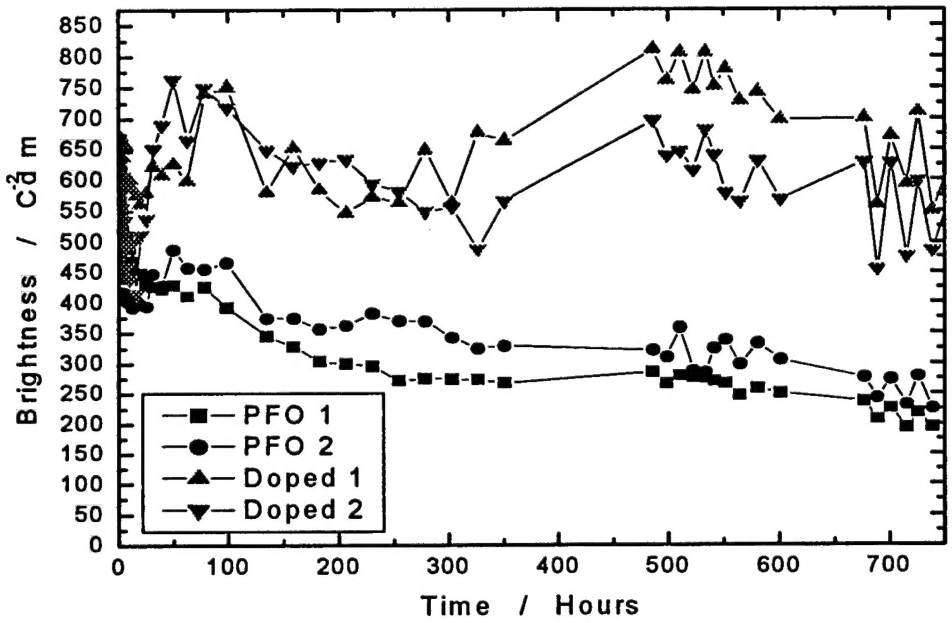

Figure 6: Shown is the brightness of two nanocomposite (red) and two pure (black) devices over a period of 750 hours. Notice the nanocomposite devices do truly live longer and remain brighter.

We have further proposed a model for this increased resistance to degradation that suggests an origin in reduced oxidation. Specifically, we suggest that this is due to triplet quenching within the system that prevents oxidation and chain scission due to ambient UV radiation. While this model is currently under study, we have preliminary data to support this point of view. Shown in figure 7 is the PL decay of PFO and PPV with and without carbon nanotubes. This singlet emission decays over time because of quenching sites induced by oxidation. The population of quenching sites is directly proportional to the population of triplets (for a given oxygen partial pressure). Thus, this measurement indirectly determines the oxidation of the polymers through the triplet population.

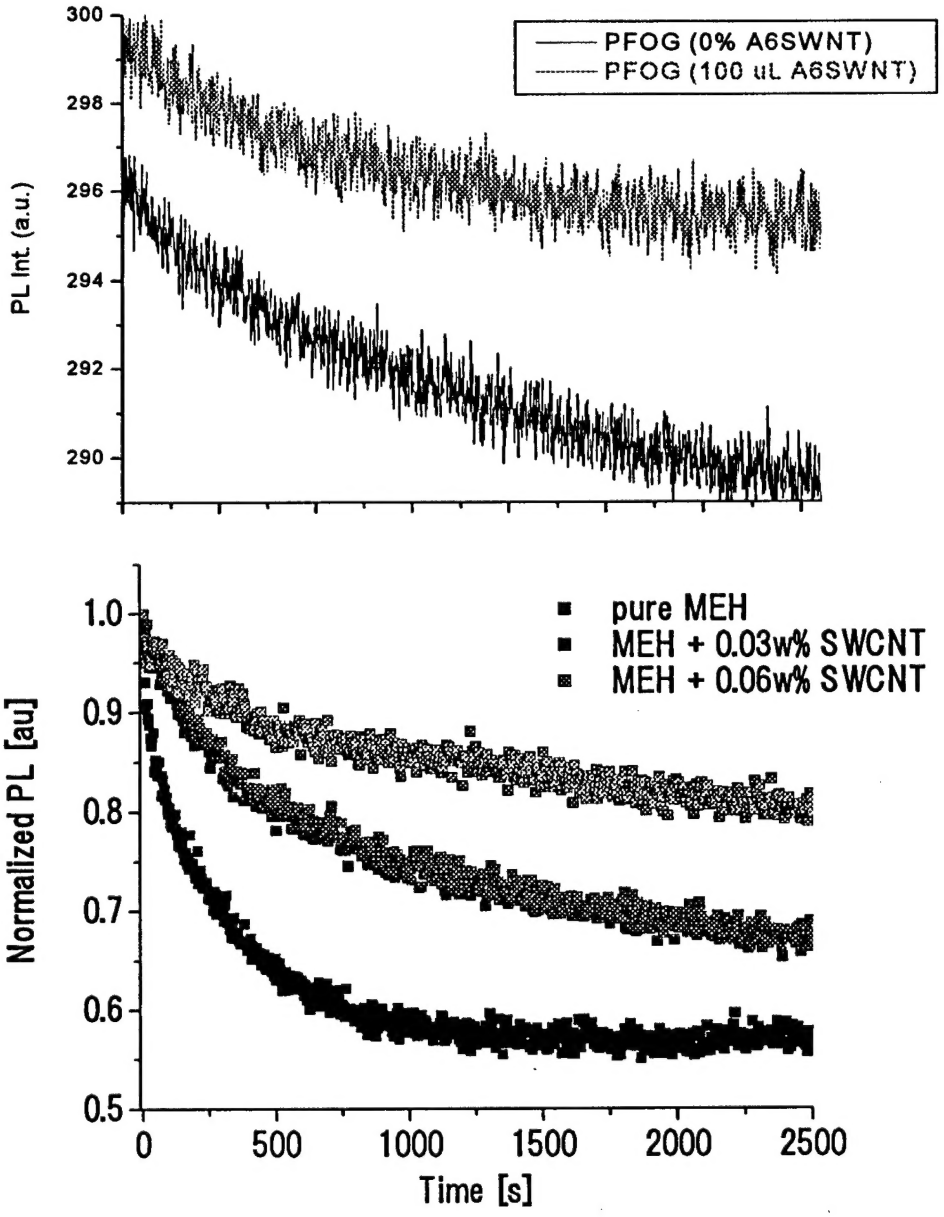

Figure 7: Decay of photoluminescence can be used as a monitor of oxidative effects in polymer-nanotube solutions. This would suggest that the nanotubes modify the overall triplet population.

Our interpretations

Preliminary spectroscopic investigations of luminescence and triplet exciton population dynamics as functions of the carbon nanotube component have been carried out to test a specific mechanism of why carbon nanotubes seem to be so effective in derailing the tendency of triplet excitons to produce oxidation damage. Although fullerene doping has shown similar tendency, the protective effect of nanotubes is much larger. Our hypothesis is an extension of the idea of Baldo et al,[1] that a mixed triplet state ($a\,\psi_T + b\,\psi_S$) of a donor can resonantly transfer its energy transfer to a fluorescent singlet state of an acceptor. Their approach, shared successfully by other groups, is to increase the singlet admixture in the triplet by incorporation of a heavy element with large H_{SO} (such as iridium) and choose the donor to have significant oscillator strength. Our experimental observation is that nanotubes introduced into a polymer host without (yet) putting in a heavy element (large H_{SO}) seems somehow to very efficiently siphon the triplets before they can do damage. Since the Baldi mechanism of resonant transfer to the singlet manifold *via* the singlet component of a mixed triplet is reasonable and attractive, we have asked what distinctive properties of nanoscale particles may influence the resonance transfer rate in a way that compensates for small b in an undoped polymer. The rate of resonant Föster transfer in the above context of mixed states is proportional to $b^2 f_D f_A$, where b has already been defined, f_D is oscillator strength of the donor, and f_A is the oscillator strength of the acceptor. In systems where the acceptor is a small fluorescent molecule, f_A is a reasonable molecular value. We advance the hypothesis that, just as in many other nanoparticle cases where excitonic states of the nanoparticle exhibit giant oscillator strengths of up to 20,000 times small molecule values (due to coherence of the electronic states over the whole nanoparticle),[2] it may be the giant coherent antenna (oscillator strength) represented by the nanotube that compensates for small b^2 in the mixed-state resonant transfer rate.

This work has been submitted for publication.

---

[1] M. A. Baldo, M. E. Thompson and S. R. Forrest, "High-efficiency fluorescent organic light-emitting devices using a phosphorescent sensitizer" Nature **403**, 750 (2000)

[2] **(a)** J. Wilkinson, K. B. Ucer, R. T. Williams, Nucl. Inst. & Meth. B (2004, in press for NIMB) **(b)** B. Gil and A. V. Kavokin, "Giant exciton-light coupling in ZnO quantum dots," Appl. Phys. Lett. 81, 748 (2002)

Novel materials for structure

Previous work in this program has developed a number of new nanomaterials for use in organic devices over the past three years. These materials are used to modify the function of the nanophase.

In this period, we report the development of two novel materials: one for use in light emitting devices and the other for use in photovoltaics. Figure 8, below, shows the wide band-gap materials developed for UV sources to be used in organic hosts. Right above are GaN nano-rods, left is shown BN nanotubes. In both cases the wide, direct transition, band-gap makes 4-5 eV light possible. Their nanoscale makes energy transfer from a host possible and allows for flexible/conformable device structures.

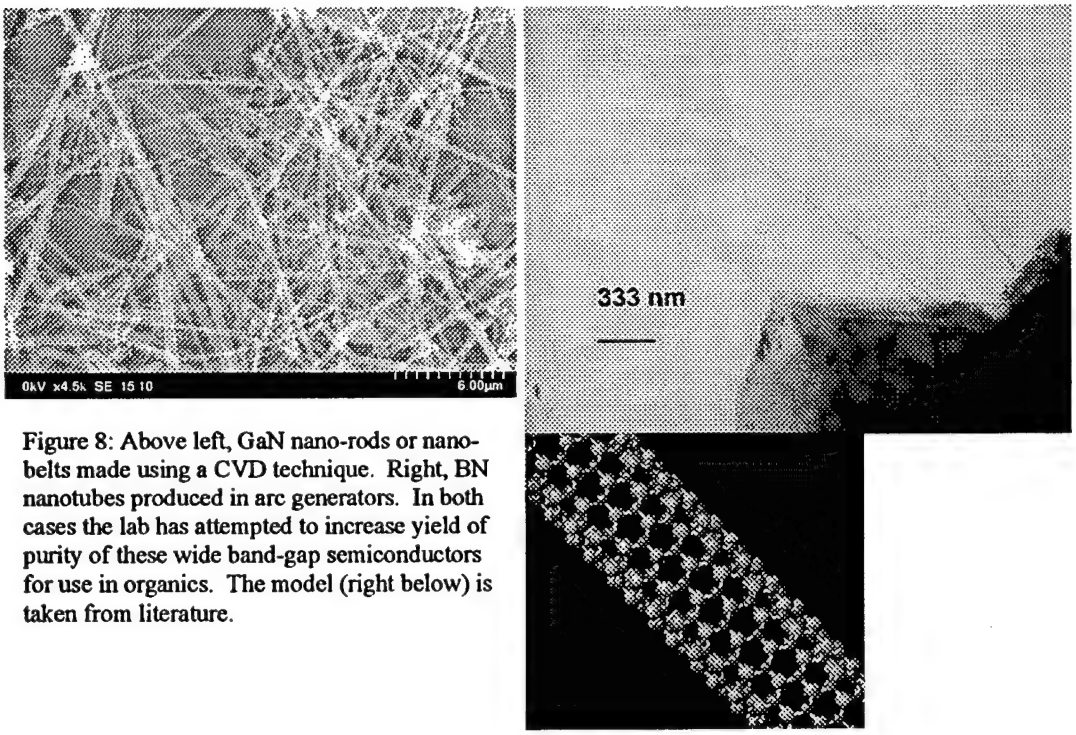

Figure 8: Above left, GaN nano-rods or nano-belts made using a CVD technique. Right, BN nanotubes produced in arc generators. In both cases the lab has attempted to increase yield of purity of these wide band-gap semiconductors for use in organics. The model (right below) is taken from literature.

A second major materials development is templated growth of conjugates polymer tubules. We have demonstrated nanotubes made from PPV and PEDOT. Shown in figure 9, PPV nanotubes are produced in large quantity using Al2O3 templates. Optical images show self-absorption in the system, thus when the tubes are unbundled they appear blue and when bundled they appear yellow green. These materials will now be filled with fullerenes to create a compact donor-acceptor system for ribust photovoltaic applications.

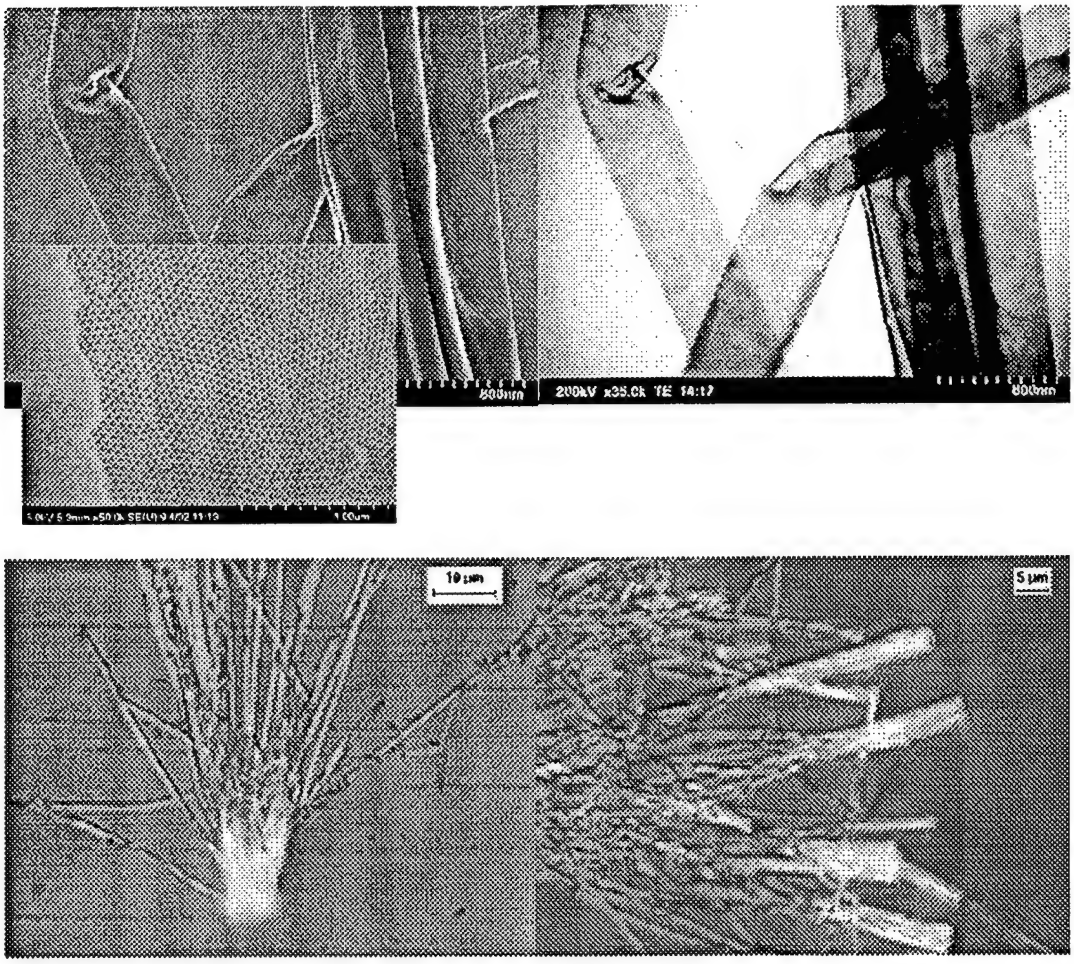

Figure 9: PPV nanotubes allow for filling and thus nano-scale donor acceptor systems can be created. Above TEM shows the tube structure and left shows the template used. Below, the optical micrographs show modification to luminescence due to self absorption phenomena.

Introducing order

Studies of Luminescent Poly(phenylene ethynylene) Coated Silica Opals were carried out in collaboration with Prof. K. Schantz at the University of Florida. In this work, we introduce the preparation of a luminescent polyelectrolyte, sulfonated Poly(phenylene ethynylene) (PPE), coated silica nanospheres constructed by the L-b-L method and their optical properties. Previous shell construction by means of a non-luminescent electrolytic polymer host blended with luminescent semi-conducting nanocrystals is advanced in this work by constructing the shell from a luminescent polyelectrolyte. Furthermore, we have prepared fluorescent opal structures from these superior core-shell structures and investigated their optical properties.

The water soluble polyconjugated polyelectrolyte PPE was chosen for the emissive material for the design of the fluorescent photonic structures. It is known that PPE has high fluorescence quantum yields, measured both in solution and in the form of thin films. Construction of the L-b-L device utilized PPE and Poly(dimethyldiallylammonium chloride) (PDDA) as the polyanionic and polycationic constituents respectively.

Absorption and photoluminescence (PL) measurements of the bilayer coated silica offer insights into the structural morphology and energy transfer within theses complexes. Polymer aggregation has been shown in these and similar species to create excimer-like states by means of inter-chain interactions. Non-aggregated PPE singlet exciton absorption (Figure 1(a) – Blue curve) is dominated by a single structure located at 425 nm with a high energy shoulder and secondary feature at 330 nm. For increasing aggregation, hence inter-chain interaction *via* π-stacking of the phenylene rings, (Figure 10(a) Green-Red-Black progressively) the main absorption feature is red shifted and a double feature develops from the singlet transition and the new molecular aggregate absorption. Non-Aggregated emission from PPE's singlet exciton (Figure 10(b) – Blue) is located around 440-450 nm with several vibrationally isolated side bands located from 460-490 nm. Emission from increasingly aggregated species (Figure 10(b) Green-Red-Black progressively) also causes a red shift by quenching the singlet excitons and the creation of an excimer-like feature around 500-600 nm.

By using the L-b-L process we have controlled the degree of aggregation by applying ultra thin bilayers on silica spheres. The deposition of PPE layers on the surface of silica spheres were verified from the absorption spectra of silica / $(PDDA/ PPE)_n$ (2×10^{-4} wt%) dispersed in ethanol (Figure 10(c)). As shown in the inset of Figure 10(c), the absorbance of PPE coated silica increased linearly with the number of the PDDA / PPE bilayer coatings. The peak absorption of the bilayers is approximately 435 nm where the morphology is in the intermediate between non-aggregated and highly aggregated. Expectedly, an increase in the number of bilayer coatings from one to five coincided with a red shift in absorption of approximately 8 nm due to aggregation. The PDDA / PPE bilayer was not observed to dissolve in the ethanol solution due to their strong electrostatic interaction. To confirm the measured linear absorption change is solely due to an increase in PPE coatings, PDDA was dissolved in ethanol and the absorption spectrum was found to be negligible and featureless in the region from 300-700 nm. Uncoated silica spheres suspended in ethanol also showed no features in this region due to their index matching.

Shown in Figure 10(d) are the relative fluorescent quantum yields of the suspended bilayer coated silica from Figure 10(c). The integrated PL was normalized by the absorbance at the excitation wavelength of 351 nm. The spectra show two main features, a weak shoulder at 460 nm originating presumably from the rapidly quenched singlet excitons and the broader excimer emission located around 500 nm indicating a slightly aggregated system. While both features are decaying exponentially (Inset of Figure 10(d)) the singlet feature is decreasing at a greater rate than the excimer exciton. The occurrence of a decaying fluorescence is expected and we believe is coincidentally

exponential. Caruso *et al* also observed aggregation and self quenching of fluorescent probes that were bound on the polyelectrolyte multilayer coated spheres and Kim *et al* reported an increase in PL efficiency of PPV nanostructures by reducing the inter-chain interaction.

In Figure 11 are non-contact AFM images of the prepared photonic crystals and their constituent uncoated and coated spheres imaged by TEM. Uncoated, 1 bilayer coating, and 5 bilayer coated structures are shown in Figures 11(a)-(c) respectively. On the micron scale, all of the prepared photonic crystals appear to be regularly packed and free from defects such as cracks occurring from solvent evaporation. TEM of the coated spheres are observed to have an increasing surface roughness as compared to the uncoated spheres indicating an increasing bilayer coating thickness consistent with the observations of the absorption measurements in Figure 10(c). The inset non-contact AFM images in Figure 11 reveal the close packing of the spheres and the possibility of the bilayer coating influence on packing. Figure 11(b) inset, (one bilayer coating) appears at first inspection to be modified by an imaging artifact perhaps caused by an asymmetric tip. Although this might be true, the optical characterization from the next section suggests that there may be additional phenomenon influencing the packing. Upon close inspection of the inset in Figure 11(c), the 5 bilayer coating appears as if the bilayer coatings are perhaps filling the voids between the spheres. This was expected due to a decreased surface stiffness of the bilayer coatings compared to the uncoated silica spheres and the bilayer coatings ability conform and infiltrate.

The optical characteristics of the PPE coated photonic crystals are shown in Figure 12. Figure 12(a) is the angle dependence of the PL and transmittance spectra from 0 – 40 degrees of a typical multicoated sphere photonic structure to the left and right respectively. The angle dependent photonic stop band is clearly observed coinciding in both measurements. The observed transmittance spectra, to the right, contains a convolution of features from the stop band, PPE absorption, scattering from the silica/PDDA coated spheres (index mismatching or dielectric contrasting), and the tail from the excimer PL. To the left in Figure 12(a), are the normalized PL spectra where the emission is significantly modified by the photonic stop band. It is also worthwhile to note the shape of the emission and what structural information this reveals. The photonic device appears to emit more similarly to the Silica/PDDA/PPE dispersions in solution in Figure 10(d) rather than the film in Figure 10(b). This suggests that during the process of forming the pseudo-crystalline structure the coated spheres were relatively undisturbed by the drying process. This is a significant observation considering one of the largest difficulties in constructing a high quality colloidal photonic crystal is maintaining a steric packing of spheres before, during, and after solvent evaporation.

Shown in Figure 12(b) are the stop band maximum positions as a function of incident angle and the relation to bilayer coatings. The solid lines are the fitted data using the familiar Bragg relation in equation 1;

$$\lambda = 2d\sqrt{2/3}\sqrt{n_{eff}^2 - n_1^2 Sin^2\theta} \qquad (1)$$

where λ is the peak Bragg wavelength, d is the sphere diameter, n_{eff} is the refractive index of the photonic crystal, and θ is the incident light angle from normal. The factor $\sqrt{2/3}$ is due to the sphere packing in a (111) geometry and n_1 is the refractive index of air. The effective refractive index of the photonic crystal (n_{eff}) was modeled by equation 2:

$$n_{eff} = \sqrt{f(n_{silica})^2 + (1-f)(n_{gap})^2} \qquad (2)$$

where f is the filling factor equal to 0.74 for this geometry, n_{silica} is the refractive index of silica equal to 1.37 at 589 nm, and n_{gap} is the refractive index of the spacing between the packed spheres referred to as the gap index. The fitted peak Bragg reflections assigned diameters of 279 nm, 285 nm, and 283 nm and a gap index of 1.10, 1.05, 1.125 for the uncoated, 1 bilayer, and 5 bilayer coatings respectively. These fitted diameters are consistent with the observations found by AFM and TEM of diameters of 280nm ±10nm in Figure 11. Although the 5 bilayer coated spheres have a fitted diameter less than the 1 bilayer coating the refractive index of the gap is greater indicating an increased filling of the 5 bilayer spheres. The anomalous behavior of 1 bilayer coating was also observed in the AFM inset micrographs in Figure 11(b). The influence on packing and the anomalous behavior of the 1 bilayer coating may be due to a fractional total coating of these spheres. In the case of 5 bilayer coatings the spheres appear to be more fully covered, hence the increasing gap index.

Further investigation of the influence of partial coatings is needed to draw significant conclusions.

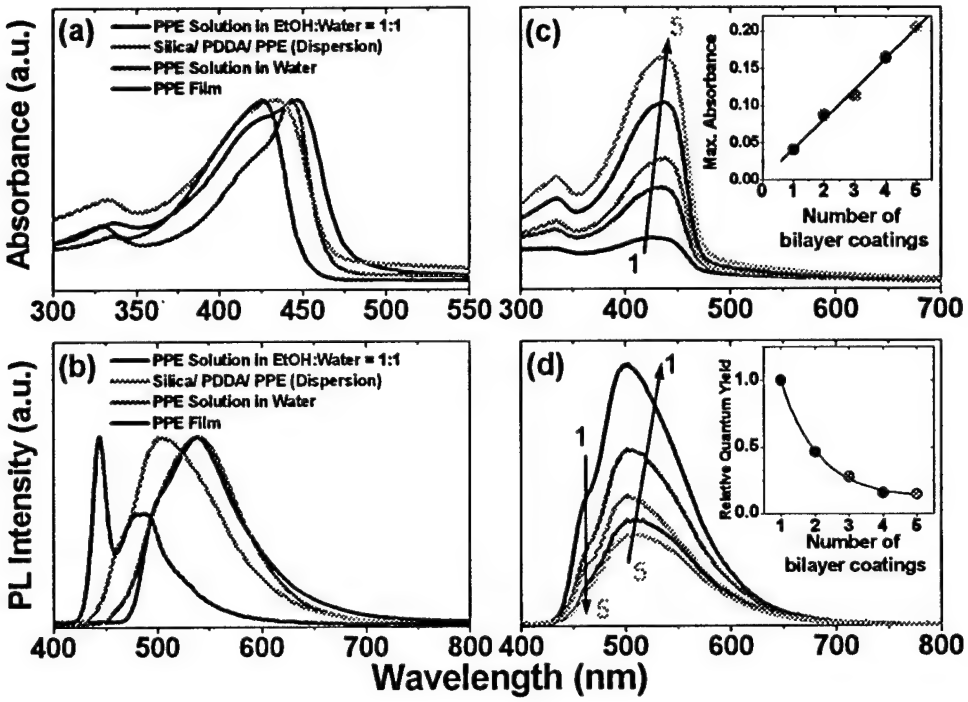

Figure 10. (a) Absorption and (b) photoluminescence spectra of PPE morphologies increasing from non-aggregated (Blue) to aggregated (Black). (c) Absorption and (d) photoluminescence spectra of $(PPE/PDDA)_n$/Silica colloidal suspensions in ethanol with increasing bilayer concentration from n equal to 1 (Black) to 5 (Cyan). Inset (c) is the linear fit to the absorption maximum in Figure 1(c) at 425 nm. Inset (d) is an exponential fit to the decreasing quantum yield in Figure 1(d) at 500 nm.

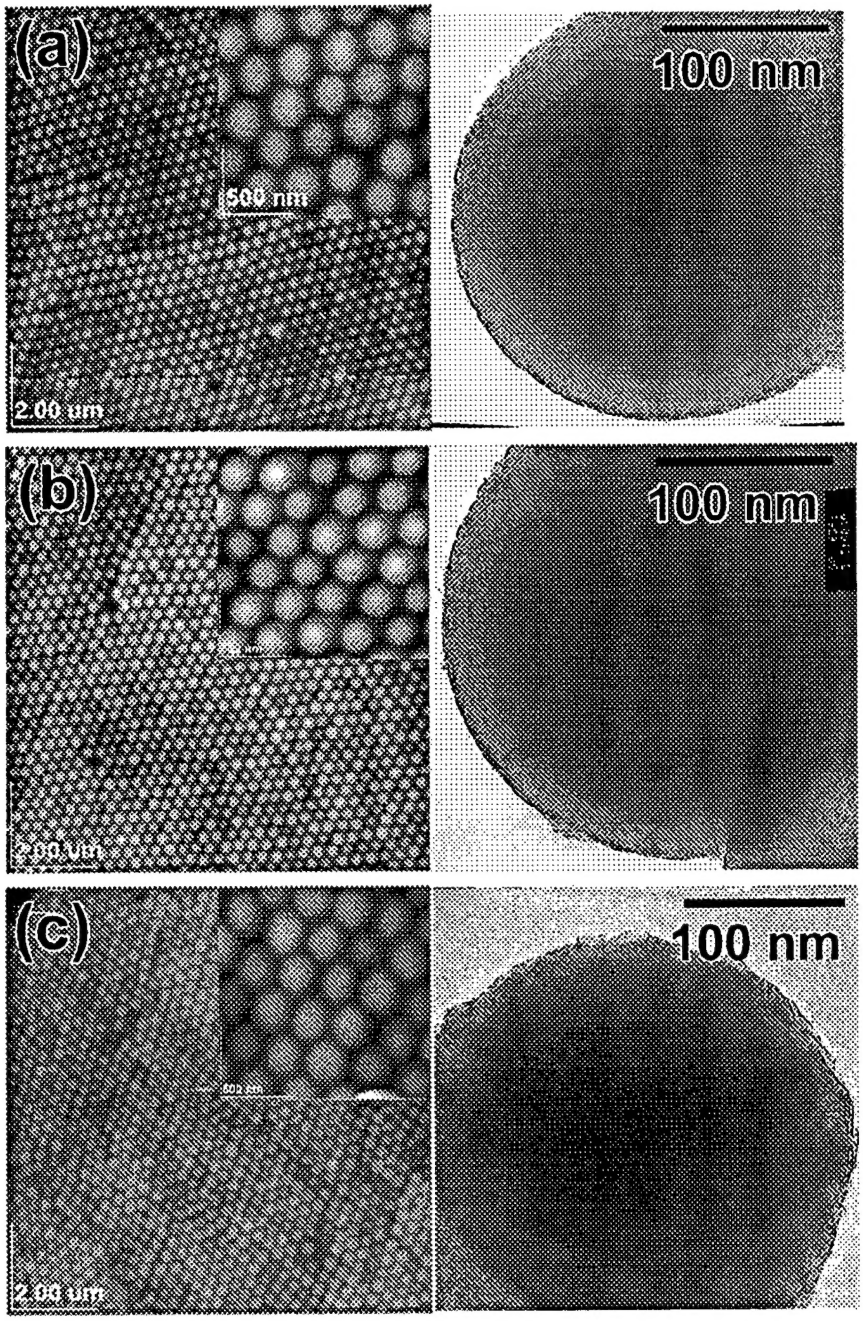

Figure 11. AFM images of the thin film photonic crystals and TEM micrographs of the constituent spheres uncoated (a), 1 bilayer (b), and 5 bilayers (c) coatings.

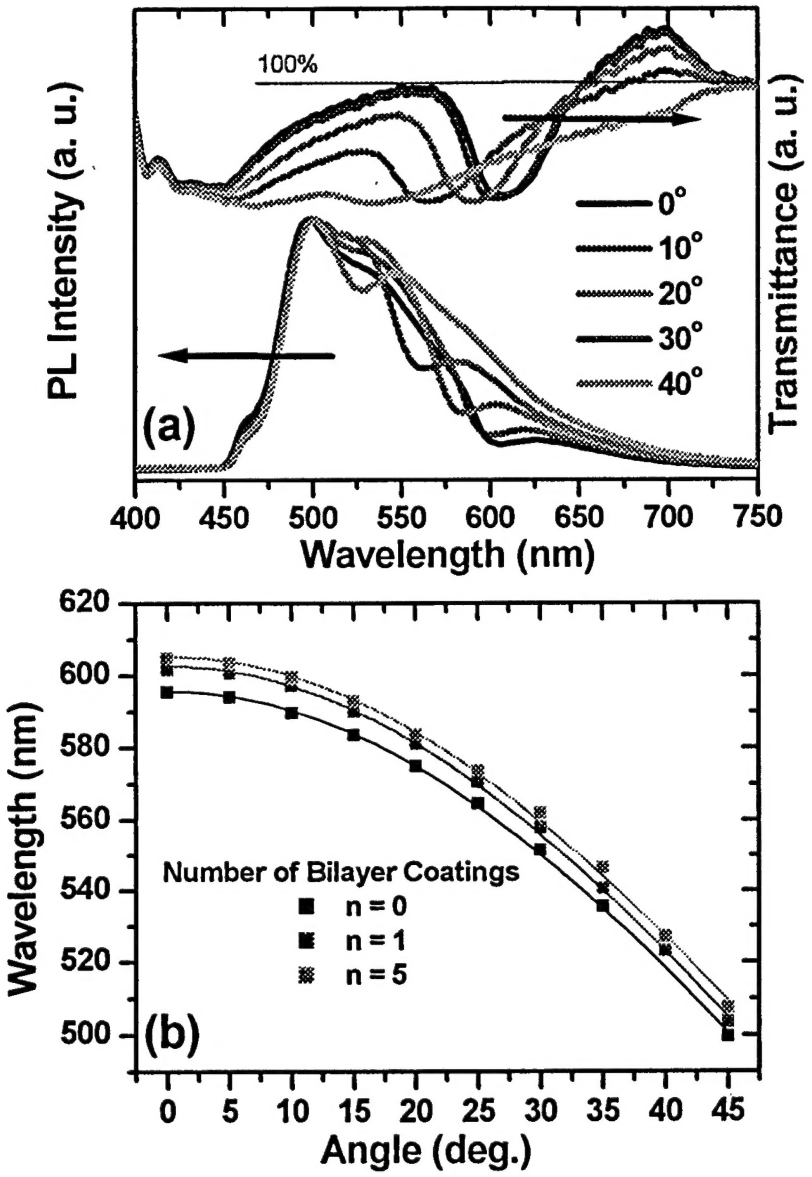

Figure 12. (a) Angle dependent transmission (Right) and photoluminescence (Left) of a typical thin film photonic crystals from 0 to 40 degrees. (b) Fitted maximum stop band wavelength verses angle for several bilayer coatings.

Performance report • F49620-03-1-0105 • "Effects of Scale-Hierarchy in *Ordered* Electro-Active Polymer Nanocomposites" • final

PAPERS

S. Webster, R. G. Grant, R. Czerw, J. Liu, M. Terrones, N. Grobert, and D. L. Carroll, "Investigation of Iron filled Nitrogen Doped Carbon Nanotubes" *(submitted to Phys. Rev. B)*

R. Czerw, S. Webster, and D.L. Carroll, "Polymer– Nanotube Composites for Transparent, Conducting Thin Films" *(in revision for JNN)*

Sihai Chen, Jianfeng Xu, Richard Czerw, and D. L. Carroll "Nanoengineering Optical Properties of Silver Nanoparticles through Shape Control" *(to be published JNN Jan 2004)*

S. Webster, J.-F. Xu, R. Czerw, J. DiMaio, J. Ballato, D. L. Carroll, and R. Nesper, "Optical Properties of Vanadium Oxide Nanotubes" (*to be published JNN Jan 2004*)

R. Czerw, P.-W. Chiu, Y.-M. Choi, D.S. Lee, D.L. Carroll, S. Roth, Y.-W. Park, " Substitutional boron-doping of carbon nanotubes" *Current Applied Physics* 2 (2002) 473-477.

M. Terrones, N. Grobert, H. Terrones, P.M. Ajayan, F. Banhart, X. Blasé, D.L. Carroll, R. Czerw, B. Foley, J.C. Charlier, "Doping and Connecting Carbon Nanotubes" *Mol. Cryst. Liq. Cryst.* Vol. 387 p 275 – 286 (2002).

S. Chen, Z. Fan, and D.L. Carroll, "Silver Nanodisks: Synthesis, Characterization, and Self Assembly", *(accepted and to be published in Journal of Chemical Physics B: Letters(2003))*

P. Tan, L. An, L. Liu, Z. Guo, R. Czerw, D.L. Carroll, P.M. Ajayan, N. Zhang, H. Guo, "Probing phonon dispersion relations of graphite from the double resonance process of antistokes Raman scattering" *(accepted and to be published in Phys Rev B (2003))*

R. Czerw, H.S. Woo, S. Webster, and D.L. Carroll, "Failure Modes in Organic Light Emitting Diodes" (*accepted and to be published in Advanced Materials* (2003))

PERSONNEL

Nicole Levi	student	Pyroelectrics
Scott Webster	student	optics
Richard Czerw	(1/2) student	devices
Jung- Ho Park	(1/2) student	PPV nanotubes
Benjamin Harrison	Postdoctoral associate	devices
J. Kim	Postdoctoral associate	photonic crystals

PATENTS

Disclosures made to Clemson University: 1

"Oxidative resistance in organic light emitting devices using carbon nanotube composites." University position has not yet been reached.

TECHNOLOGY TRANSITION

Our lab is continuing to develop a relationship with Foster-Miller (contact Tom Tiano) in Waltham MA. Specifically, we are developing applications for doped nanotubes through an SBIR program with that company.

We have also provided EIC in Boston MA (contact David Rauh) with silver nanoparticles for an SBIR in surface enhanced Raman detectors.

Both of these materials have been developed due to the AFOSR program.

FINALLY

August 15, 2003, the research group moved to Wake Forest University. The University has provided the group with more that 1.5 million in infrastructure including high resolution microscopy, a clean room for organic device fab, a new scanning probe microscope and access to fs laser spectroscopy. The newly renovated facility is dedicated to nanosciences and fully equipped to carry out the studies of this program. Along with additional support provided by Wake, the whole of the equipment base along with all personnel of the group moved to Wake.

Shown right is an organic light emitter in the form of our new home university seal.

End of report